Bladeless-Turbine-Based Triboelectric Nanogenerator for Fluid Energy Harvesting and Self-Powered Fluid Gauge

*Jian Chen, Wei Tang, Kai Han, Liang Xu, Baodong Chen, Tao Jiang, and Zhong Lin Wang**

Triboelectric nanogenerator (TENG) is attractive as an energy harvesting and self-powered sensing technology. The working frequency and surface charge density are the key factors that influence the output performance. To boosting the output of the TENG by improving the working frequency, a bladeless turbine–based triboelectric nanogenerator (BT-TENG) is designed, which transforms the fluid flow into a high rotation motion that drives the rotation TENG. When blown by compressed air, the BT-TENG rotates at an average speed of 7500 rpm. Owing to its high-frequency rotation, the short-circuit current of the BT-TENG is 60 μA and the output power is 3.6 mW. By integrating six layers of TENG into the bladeless turbine (BT-6TENGs), the total short-circuit current is 180 μA and the output power reaches 15 mW. The BT-6TENGs could charge a 4.7 mF capacitor to 3.6 V within 3 min, and continuously drive a wireless sensor to collect data and transmit to a smartphone. In practical applications, the BT-TENG could harvest steam mechanical energy, which can be widely used in home heat steam to industrial wasted heat. Additionally, the BT-TENG is integrated within a fluidic system as a self-powered flow rate sensor.

1. Introduction

Since its first invention in 2012,[1] triboelectric nanogenerator (TENG) has drawn extensive attention. Conventionally, the operational principle of TENG relies on the coupling effect of triboelectrification and electrostatic induction.[2–4] It can convert ambient mechanical energy from various sources, such as wind,[5] human body motion,[6] and ocean wave,[7,8] into useful electrical energy. The TENG shows a great potential as self-powered active sensors with applications including wearable electronics,[9,10] infrastructure monitoring,[11] and medical science.[12] There are also the advantages of cost-effective, simple fabrication, and high efficiency.

The critical challenge for the practical applications of TENG is relatively low output power, which is determined by the surface charge density and the working frequency. Several methods have been developed to increase the charge density on the dielectric surface, such as corona charging and charge pump.[13–17] However, the surface charge density is limited to a relatively low value because of air breakdown.[18] On the other hand, increasing the working frequency of the TENG is found to be a feasible method for improving the current.[19–22] As a typical structure, the rotational disk-based TENG has been widely studied. Owing to the nonintermittent and ultrafast rotation-induced charge transfer, it achieves a very high sinusoidal current output performance. Driven by powerful electromotors and complicated gear system, the rotation speed of the TENG reaches several hundred rpm and even 1000 rpm. But it is hard to increase the frequency further, because of the structure and the material strength.[23,24] However, the bladeless turbine is reported to have advantages of very high rotation speed, simple fabrication, easy maintain, as well as wide selection of materials.[25–28] Here, we combine a bladeless turbine with triboelectric nanogenerator (BT-TENG), which transforms the fluid flow into rotation motion and generates electrical output. It can achieve high rotation speed without electromotors. When blown by compressed air at pressure of 48 kPa, the BT-TENG rotated at ≈7500 rpm, which is about eight times faster than those reported in previous literature.[29,30] Thanks to its high-frequency rotation, the short-circuit current reached 63 μA, and the output power was 3.6 mW. Due to the planar structure of both the turbine and TENG, it is very easy to integrate multiple layer TENG on the whole system. When six TENGs were integrated with the bladeless turbine coaxially, the total short-circuit current was up to 180 μA and the output power increased to 15 mW, which is

J. Chen, Prof. W. Tang, K. Han, Prof. L. Xu, Prof. B. D. Chen, Prof. T. Jiang, Prof. Z. L. Wang
CAS Center for Excellence in Nanoscience
Beijing Key Laboratory of Micro-Nano Energy and Sensor
Beijing Institute of Nanoenergy and Nanosystems
Chinese Academy of Sciences
Beijing 100083, P. R. China
E-mail: zhong.wang@mse.gatech.edu

J. Chen, Prof. W. Tang, K. Han, Prof. L. Xu, Prof. B. D. Chen, Prof. T. Jiang, Prof. Z. L. Wang
School of Nanoscience and Technology
University of Chinese Academy of Sciences
Beijing 100049, P. R. China

Prof. Z. L. Wang
School of Materials Science and Engineering
Georgia Institute of Technology
Atlanta, GA 30332-0245, USA

The ORCID identification number(s) for the author(s) of this article can be found under https://doi.org/10.1002/admt.201800560.

DOI: 10.1002/admt.201800560

sufficient to operate wireless-sensing devices. As a demo, the BT-6TENG was used to continuously power a wireless Bluetooth pedometer to collect data and transmit to a mobile phone. In practical applications, the BT-TENG could harvest steam energy from household water boiler and industrial wasted heat. Furthermore, the BT-TENG could be integrated within fluidic system as a self-powered flow rate sensor.

2. Basic Structure and Working Mechanism of BT-TENG

The basic structure of the BT-TENG mainly consisted of two functional parts, the bladeless turbine and the triboelectric nanogenerator, as schematically illustrated in **Figure 1**a. The rotator of the bladeless turbine was simply made up of a series of flat, closely spaced, co-rotating disks, which could be made by stacking up steel disks, or 3D-printing items. The triboelectric nanogenerator consisted of two parts, the dielectric disk that was covered with fan-shaped polytetrafluoroethylene (PTFE) film, and the electrodes plate with complementary electrodes.

The working fluid is injected from the side wall of the case. The fluid passes through the narrow gaps between the disks, and approaches spirally toward the exhaust ports, as indicated by the red arrow heads in Figure 1a. Due to the viscous effects on the boundary layer at the surfaces of the parallel disks, the fluid then transfers its momentum to the driving torque of the disks. The resultant force of all the disk causes the rotor to rotate.[31,32] The stream lines and the velocity distribution of the boundary layer are shown in Figure 1b, which are simulated by COMSOL software. When the bladeless turbine rotates, the fan-shaped PTFE film slides on the electrodes plate and generates electricity. Figure 1c depicts the charge transfer process of the BT-TENG under short-circuit condition. The surface of PTFE is negatively charged by triboelectrification between the copper electrodes. At step I, the PTFE film is at the overlapped position of electrode A and it will induce positive charges on it. When the fan-shaped PTFE film slides from electrode A toward electrode B, the positive charges in the loop will flow from electrode A to electrode B via the load to screen the local field of the nonmobile negative charges on the PTFE film (step II). When the PTFE film reaches the overlapping position of electrode B, all the positive charges will be driven to electrode B (step III). This is regarded as the first half-cycle of electricity generation. After that, as the PTFE film keeps moving, it continues to slide from electrode B toward electrode A, a reversed current is formed. This is the second half-cycle of the electricity generation process.

To characterize the electrical output performance of the BT-TENG, an air compressor system with a barometer and a pressure control valve was established to produce the fluid flow. Here, the electrodes and the PTFE film were divided into two segments (semicircle structure), and the inlet fluid pressure was set at 48 kPa. As is shown in **Figure 2**a,b, the open-circuit voltage was 230 V and the short-circuit current was 16 μA. The transferred charge was 70 nC and the charge density was 32 μC m^{-2}. The rotation speed was obtained by counting the number of the pulse signals of the electric output of the TENG. The frequency of the electric output was 125 Hz, so that the

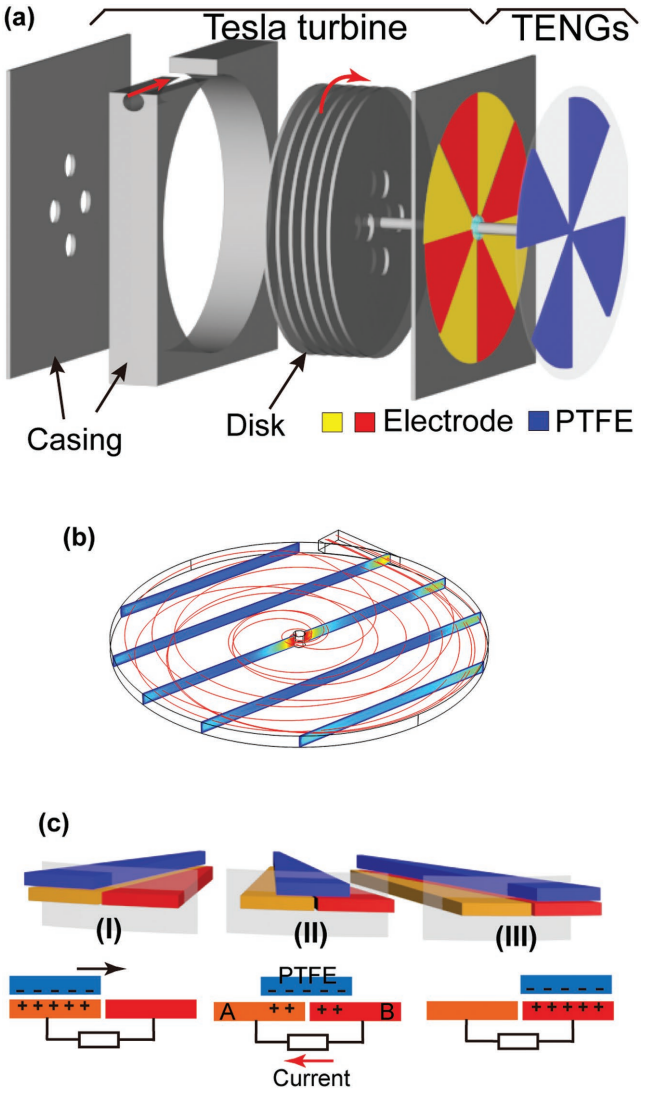

Figure 1. Structural design of the blade-less turbine–based triboelectric nanogenerator (BT-TENG) and the working principle. a) Schematic illustrations of the BT-TENGs. The air flows tangentially into case and enters the inner space between the disks (indicated by the red arrow), causing the turbine to rotate. Through the shaft, the rotation transmits to the free-standing TENG and output energy. b) The COMSOL simulation of fluid inside the gap. The streamline shows that the fluid approaches spirally toward the exhaust port. The sectional view is the velocity distribution. c) The principle of the TENG: I) the initial state in which the rotator is in alignment with electrode A. The bottom sectional view illustrates charge distribution and current. II) Intermediate state in which the rotator is moving away from electrode A toward electrode B. III) Final state in which the rotator is in alignment with electrode B.

rotation speed of the turbine was 7500 rpm, which is about eight times faster than previous literature.[30,33,34] Figure 2c shows that the output current and power were affected by the load resistance in the BT-TENG. Various load resistors were connected to the BT-TENG, and the output current and power across the resistor were measured under condition at a working frequency of 125 Hz. The amplitude of the output current was almost unchanged when the load resistance less than 100 kΩ, which was approximately the short-circuit current.

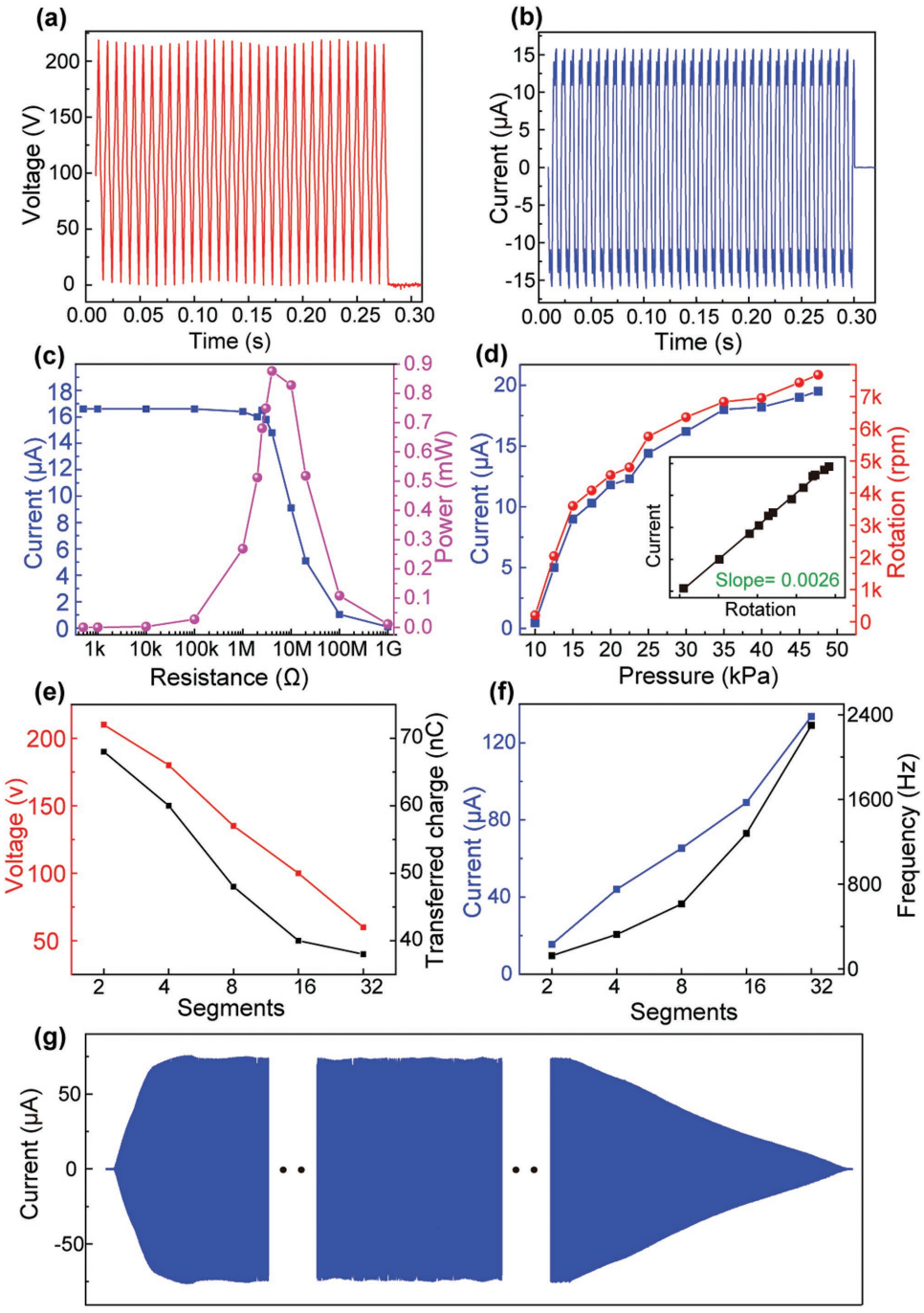

Figure 2. Electrical output performance of the BT-TENG. a) Open-circuit voltage (*Voc*). b) Short-circuit current. c) Load matching test. Maximum output power was 0.9 mW, obtained at the matched load of 6 MΩ. d) Short-circuit current and rotation rate of the BT-TENG at different gas pressures. The inset shows the linear fitting of the rotation speed and the output current. e) The open-circuit voltage and transferred charge of the BT-TENGs when the electrode was divided into different segments. f) The short-circuit current and the working frequency of BT-TENGs when the electrode was divided into different segments. g) The durability test of the BT-TENG.

The measured maximum output power was 0.9 mW with the matched resistance of 6 MΩ.

The inlet pressure is the main influencing factor of the turbine rotation.[35] Experiments were carried out to investigate how the inlet pressure affects the rotation speed and the output performance of the TENG. The result is shown in Figure 2d. When the inlet pressure was less than 10 kPa, the BT-TENGs could not rotate at all due to the frictional resistance. The transition happened at 13 kPa, and the BT-TENG suddenly started rotating very quickly with the speed of 2000 rpm and the short-circuit current reached 5 μA. This is possibly because the sliding friction force is smaller than the static friction force.

When the inlet pressure generally increased from 15 to 48 kPa, the rotation speed also increased from 3600 to 7500 rpm and the short-circuit current increased from 8 to 18 μA. When the inlet pressure exceeded 60 kPa, the rotation speed was higher than 12 000 rpm. But the BT-TENG was very unstable because it was beyond the mechanical strength limit in our experiments. As shown in the inset of Figure 2d, the short-circuit current was linearly related to the rotation speed and could be numerically fitted well by a formula: $I = 0.0026 \times R - 0.2035$, where I is the short-circuit current and R is the rotation speed. This illuminates its potential application as self-powered angular speed sensor or fluid gauge. The open-circuit voltage was 230 V and did not change with the rotation speed or the inlet pressure.

To enhance the electric output, the PTFE and electrodes were divided into several segments. As the number of segments (N) increasing from 2 to 32, the open-circuit voltage decreased from 230 to 60 V, and the transferred charge decreased from 68 to 38 nC (Figure 2e). This tendency may result from the fact that the finer segments only need smaller separation distance and so the lower magnitude of polarization.[34] The output current of the BT-TENG increased from 18 to 138 μA and the working frequency of TENG increased from 125 to 2300 Hz, as illustrated in Figure 2f. When the TENG was divided into eight segments, the output power reached the maximum of 3.6 mW under the matched impedance of 3 MΩ. The matched impedance was decreased compared to that in Figure 2c, because the frequency was increased. The rotating speed of the turbine kept at ≈8000 rpm with small fluctuation under the condition of an inlet pressure of 48 kPa. In addition, this optimized structure will be used in the following sections.

Additionally, the enduring test of the optimized BT-TENG device was also conducted. The result is shown in Figure 2g. When blown by air, the BT-TENG started rotating and the rotation speed accelerated very quickly. Accordingly, the frequency and amplitude of the current increased quickly. After 13 s, the rotation of the turbine has accelerated to the maximum speed, which was about ≈8000 rpm. And so, the current of the BT-TENG reached the maximum of ≈60 μA. Then, the BT-TENG kept running as long as the inlet air pressure kept stable. After 4 min, the air blown was stopped. The BT-TENG kept running due to the inertial momentum, but the speed was generally decelerated because of the friction force. The current decreased generally as the rotation speed slowing down the rotation of the BT-TENG stopped after another 60 s. According to the equation

$$\alpha_1 = \Delta\omega_1/\Delta t_1, \quad \alpha_1 = (M_1 - M_2)/I_1 \tag{1}$$

$$\alpha_2 = \Delta\omega_2/\Delta t_2, \quad \alpha_2 = M_2/I_2 \tag{2}$$

Here, α is the angular acceleration, ω is the angular speed, Δt is the time different, M is the torque, and I is the rotational inertial. "1" represents the acceleration process and "2" represents the deceleration process. The deceleration time Δt_2 was ≈60 s, about five times longer than the acceleration time Δt_1, ≈13 s. This means that the driving torque was about six times larger than the friction torque. So, a single bladeless turbine can drive more than one TENG and contribute to a multiplied power output. Thanks to the planar structure of this BT-TENG, it is very easy to integrate many TENGs on a single turbine. As is shown in **Figure 3**a, the electrodes' plate and the dielectric disk of the new TENGs were coaxially stacked on the shaft.

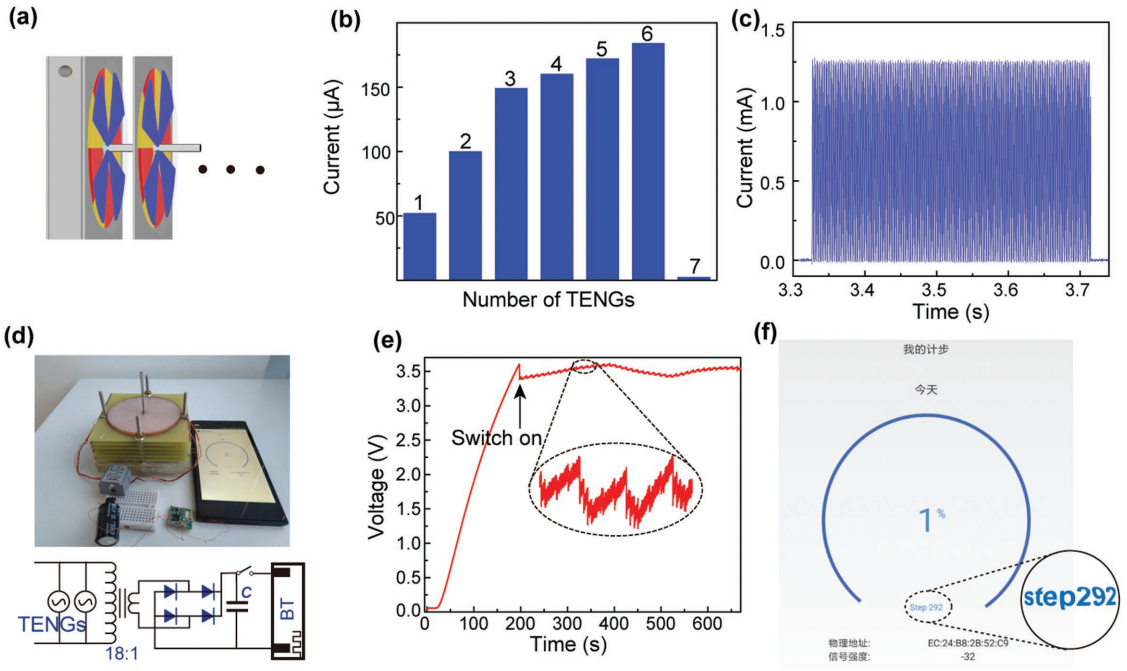

Figure 3. Applications of BT-6TENGs. a) Illustration of several TENGs stacked up coaxially on single bladeless turbine. b) The short-circuit current of the system when a different number of TENGs were stacked on single bladeless turbine. c) Short-circuit current of the BT-6TENGs after step down and rectified. d) The photograph of the self-powered wireless Bluetooth pedometer and the circuit diagram. e) The voltage of the capacitor. f) The screenshot of the app in mobile phone.

Both the electrodes and dielectric of different TENGs were aligned to make sure the phase alignment. So, the electrodes could be directly connected in parallel to enhance the current output. As is shown in Figure 3b, the short-circuit current doubled from 50 to 100 μA when two TENGs were stacked on parallelly. The short-circuit current reached up to 150 μA when three TENGs were stacked on. The average current of each TENG kept unchanged, which indicated that the rotation speed of the turbine did not change. As more TENGs were stacked on, the total current increased a little. But the average current of each single TENG decreased due to the rotation being slowing down. When six TENGs were stacked on the shaft, the short-circuit current of the BT-6TENGs was about 180 μA. The current of each single TENG was only 30 μA in average, which was significantly reduced. When seven TENGs were stacked on, the total friction torque was larger than the driving torque. So, the BT-7TENGs could not rotate at all and the output directive decreased to zero. This result conforms to the calculation result in Equation (1) that the driving torque is nearly six times larger than the friction resistance torque. The whole system of the BT-6TENGs was 10 cm by 10 cm by 5 cm in size and the total output power was ≈15 mW or 30 W m^{-3}. The high-output performance of this BT-6TENGs makes it able to power the internet of thins (IOT) electronic devices, such as a wireless Bluetooth pedometer. A step-down transformer with a ratio of 18:1 and a bridge rectifier were used as a power-management unit. Finally, the device's DC current output reaching up to 1.25 mA and the open-circuit voltage was 7 V, as is shown in Figure 3c. A 4.7 mF/16 V capacitor was chosen as the storage component.[36–38] The wireless Bluetooth pedometer was attached to a pendulum and swung as the pendulum. The photograph of the system and the equivalent circuit are given in Figure 3d. When blown by air, the BT-6TENGs started working. The 4.7 mF capacitor was charged very quickly to 3.6 V within 150 s (Figure 3e). Then we turned on the pedometer. And it can be seen from Figure 3e, the wireless pedometer consumed more energy than that the BT-6TENGs could generate, leading to a very small voltage drop of the capacitor. After the Bluetooth switching into the sleep mode, the BT-6TENGs generated more energy than the wireless pedometer consumed. So, the capacitor stored energy and the voltage returned to ≈3.5 V. The interval of the voltage rising and falling was ≈10 s, which meets the working frequency of the Bluetooth. The whole device was working well for about 10 min (Figure 3e). The long cycle of the fluctuation may be the fluctuation of the inlet pressure. An android mobile app was developed to receive the signal by Bluetooth and the data are shown in the screen capture image in Figure 3f.

In a practical application, the BT-TENG could be widely used in energy harvesting from the common water boiler and industrial wasted heat. As is shown in **Figure 4**a, the water boiler was preheated about 5 min to generate high pressured steam. The steam drove the BT-TENG rotating and generating electricity. The short-circuit current was 30 μA and open-circuit voltage was 120 V. The hot steam drove BT-TENG could light up a flashlight or charge the capacitor.

There is also possibility of using BT-TENG as self-powered fluid gauge. From the inset of Figure 2d, the output current of the BT-TENGs was directive related to the rotation speed. And the rotation speed was determined by the fluid volume. To integrate the BT-TENG into the pipeline and improve the sensitivity, a tiny scale 3D-printed bladeless turbine was used to drive the TENG. The individual components and the assembled device are shown in Figure 4b. The output current was linearly

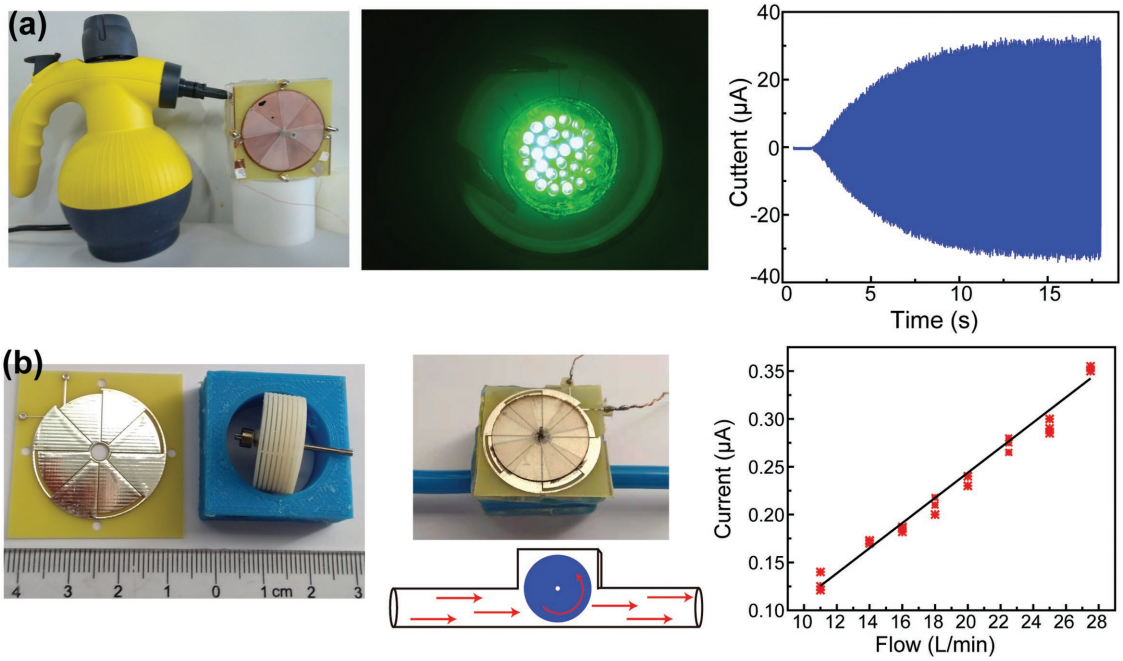

Figure 4. Applications of the BT-TENG. a) The photograph of the BT-TENG that was drove by a water boiler and it could light up a torch and the short-circuit current was up to 30 μA. b) The mini scale BT-TENG that was fabricated by 3D printing. It can be used as self-powered fluid gauge; the current performance was linearly related to the flow.

increase from 0.125 to 0.35 μA as the fluid volume increase from 11 to 28 L min^{-1}. Such a simple and low-cost self-powered fluid gauge could be used to build the smart home.

3. Conclusion

In summary, we demonstrated a BT-TENG with advantages of simple fabrication, high working frequency, and high-output performance. Under the inlet pressure of 48 kPa, the rotation speed was as high as 7500 rpm, which was about eight times faster than that reported in other literatures. The maximal output power of the optimal BT-TENG was ≈3.5 mW at a load resistance of 3 MΩ. By coaxially stacking up six TENGs on the bladeless turbine, the device's output reached 15 mW and could continuously power a wireless Bluetooth pedometer to collect and transmit data to a mobile phone. It is promising to apply the BT-TENG for several potential applications, such as harvesting energy from a water boiler and industrial waste heat. The tiny BT-TENG can also serve as self-powered fluid gauge for smart home and city.

4. Experimental Section

Bladeless Turbine: For the rotator of the bladeless turbine, 300 μm stainless steel was used and cut into the disks by using a laser cutting machine. Then the disks were stacked parallelly on the shaft through the central hole and spaced by the four thick tiny spacers at the rim. Rivets were used to fix the disks and spacers through the positioning point. The case was made of acrylic by laser cutting.

Triboelectric Nanogenerator: The electrodes were fabricated on copper clad FR4 plate by printed circuit board (PCB) manufacturing processes. The circular Cu layer was divided fan-shaped electrodes into two groups with the same shape, where the electrodes from different groups were alternately arranged with 0.2 mm gaps to insulate them. The electrodes' plate was fixed on the case and kept static, while the shaft went through the plate from the central hole. As for the free-standing dielectric disk, the PTFE film (thickness ≈80 μm) was fixed on a 0.3 mm FR-4 disk and the PTFE was cut into fan-shaped as same as the shape of electrode A. This dielectric disk was fixed on the shaft and rotated as it. Finally, the as-prepared parts were assembled into a whole device by means of screws, springs, bearings, and seal ring.

Measurement Setup: An electrometer (Keithley 6514) with a Data Acquisition Card (NI PCI-6259) was used to measure the short-circuit current and transferred charge. The rotation speed was obtained by counting the frequency of the sine wave signals. Moreover, a Keithley oscilloscope was used to test the open-circuit voltage.

Acknowledgements

J. Chen and W. Tang contributed equally to this work. Research was supported by the National Key R&D Project from Minister of Science and Technology (2016YFA0202704), Beijing Municipal Science & Technology Commission (Z171100000317001, Z171100002017017, Y3993113DF), National Natural Science Foundation of China (Grant Nos. 51432005, 5151101243, and 51561145021). Patents were filed based on the research results presented in this manuscript.

Conflict of Interest

The authors declare no conflict of interest.

Keywords

bladeless turbines, fluid energy, fluid gauge, high speed, triboelectric nanogenerators

Received: October 26, 2018
Revised: November 14, 2018
Published online:

[1] F. R. Fan, Z. Q. Tian, Z. Lin Wang, *Nano Energy* **2012**, *1*, 328.
[2] Z. L. Wang, *ACS Nano* **2013**, *7*, 9533.
[3] Z. L. Wang, J. Chen, L. Lin, *Energy Environ. Sci.* **2015**, *8*, 2250.
[4] Z. L. Wang, *Mater. Today* **2017**, *20*, 74.
[5] A. Ahmed, I. Hassan, M. Hedaya, T. Abo El-Yazid, J. Zu, Z. L. Wang, *Nano Energy* **2017**, *36*, 21.
[6] X. Wang, Y. Yin, F. Yi, K. Dai, S. Niu, Y. Han, Y. Zhang, Z. You, *Nano Energy* **2017**, *39*, 429.
[7] L. Xu, Y. Pang, C. Zhang, T. Jiang, X. Chen, J. Luo, W. Tang, X. Cao, Z. L. Wang, *Nano Energy* **2017**, *31*, 351.
[8] Z. L. Wang, T. Jiang, L. Xu, *Nano Energy* **2017**, *39*, 9.
[9] S. Li, J. Wang, W. Peng, L. Lin, Y. Zi, S. Wang, G. Zhang, Z. L. Wang, *Adv. Energy Mater.* **2017**, *7*, 1602832.
[10] J. Deng, X. Kuang, R. Liu, W. Ding, A. C. Wang, Y.-C. Lai, K. Dong, Z. Wen, Y. Wang, L. Wang, H. J. Qi, T. Zhang, Z. L. Wang, *Adv. Mater.* **2018**, *30*, 1705918.
[11] L. Jin, W. Deng, Y. Su, Z. Xu, H. Meng, B. Wang, H. Zhang, B. Zhang, L. Zhang, X. Xiao, M. Zhu, W. Yang, *Nano Energy* **2017**, *38*, 185.
[12] Q. Zheng, Y. Zou, Y. Zhang, Z. Liu, B. Shi, X. Wang, Y. Jin, H. Ouyang, Z. Li, Z. L. Wang, *Sci. Adv.* **2016**, *2*, 1.
[13] W. Tang, T. Jiang, F. R. Fan, A. F. Yu, C. Zhang, X. Cao, Z. L. Wang, *Adv. Funct. Mater.* **2015**, *25*, 1.
[14] Z.-H. Lin, Y. Xie, Y. Yang, S. Wang, G. Zhu, Z. L. Wang, *ACS Nano* **2013**, *7*, 4554.
[15] J. Chun, B. U. Ye, J. W. Lee, D. Choi, C.-Y. Kang, S.-W. Kim, Z. L. Wang, J. M. Baik, *Nat. Commun.* **2016**, *7*, 12985.
[16] J. Wang, C. Wu, Y. Dai, Z. Zhao, A. Wang, T. Zhang, Z. L. Wang, *Nat. Commun.* **2017**, *8*, 1.
[17] L. Xu, T. Z. Bu, X. D. Yang, C. Zhang, Z. L. Wang, *Nano Energy* **2018**, *49*, 625.
[18] Y. Zi, C. Wu, W. Ding, Z. L. Wang, *Adv. Funct. Mater.* **2017**, *27*, 1700049.
[19] C. Wu, R. Liu, J. Wang, Y. Zi, L. Lin, Z. L. Wang, *Nano Energy* **2017**, *32*, 287.
[20] G. Zhu, J. Chen, T. Zhang, Q. Jing, Z. L. Wang, *Nat. Commun.* **2014**, *5*, 3426.
[21] Q. Tang, M.-H. Yeh, G. Liu, S. Li, J. Chen, Y. Bai, L. Feng, M. Lai, K.-C. Ho, H. Guo, C. Hu, *Nano Energy* **2018**, *47*, 74.
[22] M. Bi, S. Wang, X. Wang, X. Ye, *Nano Energy* **2017**, *41*, 434.
[23] J. Wang, W. Ding, L. Pan, C. Wu, H. Yu, L. Yang, R. Liao, Z. L. Wang, *ACS Nano* **2018**, *12*, 3954.
[24] J. Bae, J. Lee, S. Kim, J. Ha, B.-S. Lee, Y. Park, C. Choong, J.-B. Kim, Z. L. Wang, H.-Y. Kim, J.-J. Park, U.-I. Chung, *Nat. Commun.* **2014**, *5*, 4929.
[25] S. Sengupta, A. Guha, *Proc. Inst. Mech. Eng., Part A* **2012**, *226*, 650.
[26] J. Song, C. w. Gu, X. s. Li, *Appl. Therm. Eng.* **2017**, *110*, 318.
[27] C. Schosser, S. Lecheler, M. Pfitzner, *Period. Polytech., Mech. Eng.* **2017**, *61*, 12.
[28] G. Manfrida, L. Pacini, L. Talluri, *Energy* **2018**, *158*, 33.
[29] Y. Xi, H. Guo, Y. Zi, X. Li, J. Wang, J. Deng, S. Li, C. Hu, X. Cao, Z. L. Wang, *Adv. Energy Mater.* **2017**, *7*, 1602397.
[30] Y. Xie, S. Wang, S. Niu, L. Lin, Q. Jing, Y. Su, Z. Wu, Z. L. Wang, *Nano Energy* **2014**, *6*, 129.

[31] A. Guha, S. Sengupta, *Eur. J. Mech. B: Fluids* **2013**, *37*, 112.
[32] M. B. Habhab, T. Ismail, J. F. Lo, *Sensors* **2016**, *16*, 1970.
[33] X. Ren, H. Fan, C. Wang, J. Ma, H. Li, M. Zhang, S. Lei, W. Wang, *Nano Energy* **2018**, *50*, 562.
[34] L. Lin, S. Wang, Y. Xie, Q. Jing, S. Niu, Y. Hu, Z. L. Wang, *Nano Lett.* **2013**, *13*, 2916.
[35] P. Lampart, K. Kosowski, M. Piwowarski, L. Jędrzejewski, *Pol. Marit. Res.* **2009**, *16*, 28.
[36] J. H. Lee, J. Kim, T. Y. Kim, M. S. Al Hossain, S.-W. Kim, J. H. Kim, *J. Mater. Chem. A* **2016**, *4*, 7983.
[37] J. Kim, J. H. Lee, J. Lee, Y. Yamauchi, C. H. Choi, J. H. Kim, *APL Mater.* **2017**, *5*, 073804.
[38] J. H. Kim, S.-W. Kim, Z. L. Wang, *APL Mater.* **2017**, *5*, 073701.

